

2006

Plasma Emission Redistribution in a Single Cycle of a Pulsed DC Magnetron

W. Zhu

Old Dominion University

G. Buyle

J. Lopez

S. Shanmugmurthy

A. Belkind

See next page for additional authors

Follow this and additional works at: https://digitalcommons.odu.edu/physics_fac_pubs

 Part of the [Plasma and Beam Physics Commons](#)

Repository Citation

Zhu, W.; Buyle, G.; Lopez, J.; Shanmugmurthy, S.; Belkind, A.; Becker, K.; and Gryse, R. De, "Plasma Emission Redistribution in a Single Cycle of a Pulsed DC Magnetron" (2006). *Physics Faculty Publications*. 40.

https://digitalcommons.odu.edu/physics_fac_pubs/40

Original Publication Citation

Zhu, W., Buyle, G., Lopez, J., Shanmugmurthy, S., Belkind, A., Becker, K., & De Gryse, R. (2006). Plasma emission redistribution in a single cycle of a pulsed dc magnetron. *New Journal of Physics*, 8. doi: 10.1088/1367-2630/8/8/146

Authors

W. Zhu, G. Buyle, J. Lopez, S. Shanmugmurthy, A. Belkind, K. Becker, and R. De Gryse

Plasma emission redistribution in a single cycle of a pulsed dc magnetron

W Zhu¹, G Buyle^{2,5}, J Lopez³, S Shanmugmurthy⁴, A Belkind⁴, K Becker^{4,6} and R De Gryse²

¹ Old Dominion University, Norfolk, VA, USA

² Ghent University, Ghent, Belgium

³ St. Peter's College, Jersey City, NJ, USA

⁴ Stevens Institute of Technology, Hoboken, NJ, USA

E-mail: kbecker@stevens.edu

New Journal of Physics **8** (2006) 146

Received 30 May 2006

Published 25 August 2006

Online at <http://www.njp.org/>

doi:10.1088/1367-2630/8/8/146

Abstract. Time-resolved images of the optical emissions from a pulsed dc titanium target planar rectangular sputtering magnetron plasma were taken using Argon spectral filters and a Roper Scientific ICCD camera with a time resolution of 0.05–0.2 μ s. At the beginning of the ‘on-time’, when the power is turned on, the discharge initially starts preferentially in two opposite curved sections (‘cross corners’) of the magnetron race track, where it exhibits the most intense plasma emissions. During the rest of the ‘on-time’, the emissions from the straight sections of the race track of the magnetron are always slightly more intense than the emissions from the curved sections of the race track. This pattern extends into the start of the ‘off-time’, when the power is turned off. In an effort to explain this ‘plasma emission redistribution (PER)’ effect, we used a Monte Carlo (MC) approach to simulate the optical emissions from our pulsed dc magnetron plasma. The simulation reproduces the PER effect, which can be linked to the specific electric (E) and magnetic (B) field spatial distributions and electric field distribution temporal variations in conjunction with the electron $E \times B$ drift.

⁵ Current address: Centexbel, Zwijnaarde, Belgium.

⁶ Author to whom any correspondence should be addressed.

Contents

1. Introduction	2
2. Experimental details	3
3. Details of the MC simulation	5
3.1. Standard MC model	5
3.2. Modification of the standard MC model	6
4. Results	8
4.1. Experimental results	8
4.2. Results from the MC simulation	9
5. Discussion	12
5.1. The early stage of a fast-rising voltage pulse	12
5.2. The steady state situation	14
6. Conclusions	14
Acknowledgments	15
References	15

1. Introduction

Sputtering magnetrons are widely used for the deposition of thin films [1]–[3]. The deposition rate and its distribution along the substrate depend on the intensity and configuration of the magnetic field that is used to confine the plasma near the magnetron target. Investigations of the relationship between the magnetic field and the plasma properties and deposition rates have allowed us to describe, predict, and tailor the deposition rate and its distribution for individual magnetrons (see [4] and references therein). These investigations were done mainly by examining steady state or averaged properties of magnetron plasmas excited by dc or RF power.

Magnetrons are now-a-days also widely used for the reactive deposition of dielectric thin films using pulsed dc power that provides the option to suppress arcing on the target and leads to more stable processes compared to continuous dc systems [5]–[9]. In a pulsed dc-driven magnetron discharge, the negative potential on the target is periodically modulated with a frequency (typically between 5 to 350 kHz) in a way that yields an ‘off-time’, during which a positive voltage (usually 10–50% of the negative voltage) is applied as part of each duty cycle. This is why the ‘off-time’ is often also called ‘reverse time’. Pulsed dc magnetron plasmas have been investigated using time-resolved Langmuir probes [10]–[14] and mass-spectrometry [15]. The first time-resolved optical emission spectroscopic (TR-OES) investigations of the pulsed dc magnetron were also reported recently [16]–[22]. Preliminary optical emission imaging studies were carried out recently to determine the effects of plasma power on the microscopic details of magnetron sputtering using pulsed dc excitation [23]. These studies provided first evidence of a plasma emission redistribution (PER) effect, i.e. the plasma emission intensity changes at the beginning of the ‘on-time’, when the plasma power is applied. During the first few tenths of a microsecond, the optical emission intensity is strongest in two opposite curved regions of the magnetron race track. Within about a microsecond after the power is applied, the emission pattern changes and the strongest emission intensity is observed coming from the straight sections of the race track. This pattern persists throughout the rest of the ‘on-time’ and into the ‘reverse-time’.

The PER effect is related to the cross-corner effect, which is an asymmetrical race track erosion that usually occurs in diagonally opposite areas of the magnetron at the point, where the straight section of the race track begins to curve [24]–[27]. We also saw such an asymmetrical erosion using various planar rectangular magnetrons and the effect coincided with an enhanced electron escape from the curved parts of the race track in experiments using magnetrons with multiple anodes. A Monte Carlo (MC) simulation using an electron temperature of 6 eV showed that the origin of the cross-corner effect is related to a difference in the strength of the magnetic field in the curved and straight sections and is most likely also related to variations in the average drift velocities of the electrons in these sections. The drift velocity increases when going from a straight section to a curved section and decreases when going from a curved section to a straight section [24].

In this paper, we present additional, more detailed experimental results elucidating the PER effect. In an effort to understand the origin of this effect, we used a MC approach. This approach consists of retracing individual electrons, i.e. for each electron the individual path, the occurring ionization, and excitation events are calculated. This MC approach is frequently used for simulating the ionization distribution in steady state dc magnetron discharges (the so-called ‘standard’ MC model, see e.g. [24]–[30]). A modified MC approach is used here to simulate the temporal evolution of the plasma emission intensity when a rapidly rising voltage pulse is applied to the magnetron. The simulation basically retraces the orbits and ionization–excitation events of the electrons that are still present in the discharge at the end of the off-time [14, 31] and that are emitted from the target.

2. Experimental details

The experiments were performed in a cubic reaction chamber (‘box coater’) with a planar rectangular magnetron HRC-373 (BOC Coating Technology) equipped with a 99.999% titanium target of size $87.2 \times 202.1 \text{ mm}^2$ (figure 1). The base pressure in the system was in the range of $4\text{--}8 \times 10^{-4} \text{ Pa}$. The working atmosphere was an Ar : O₂ mixture at a gas flow ratio of 1 : 1 and a pressure of 1.2 Pa. The images were taken by placing a Roper Scientific ICCD camera (controlled by an ST-133 controller) directly at the viewing window, which is located at the centre of the front of the chamber (figure 1). A mirror was placed under the magnetron to reflect the full view of the image of the magnetron to the viewing window.

The magnetic field of the magnetron was characterized with a MPS GM/X Gaussmeter to determine the distribution of the component of the magnetic induction parallel to the target surface, B_{\parallel} . This component determines the plasma confinement in the race track area. It was measured along the centre line of the race track at a distance of about 1.5 cm from the target surface, which corresponds to the region of the most intense magnetron plasma. The centre line of the race track was determined by the condition that $B_{\perp} = 0$, where B_{\perp} is the component of the magnetic field induction normal to the surface (figure 2). In the curved regions, the component B_{\parallel} of the magnetic induction is in the range 60–70 Gauss, while it is in the range 80–90 Gauss along the straight sections. The variation of the component B_{\parallel} with the distance z from the target surface is shown in the side graphs of figure 2.

The pulsed dc power was provided by a combination of an Advanced Energy[®] MDX-10 dc power supply and an Advanced Energy[®] Sparc-le V pulse generator. The pulsed dc power supply system was operated in the constant power mode at a power of 1 kW, repetition frequency of

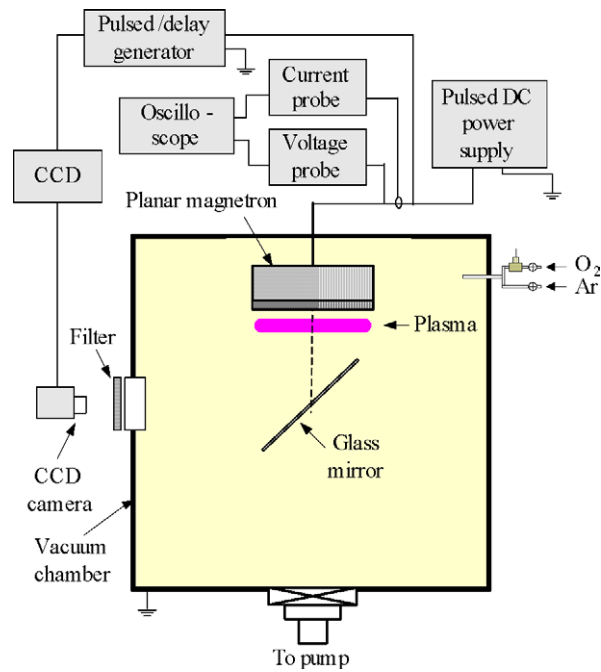


Figure 1. Schematic diagram of experimental set up.

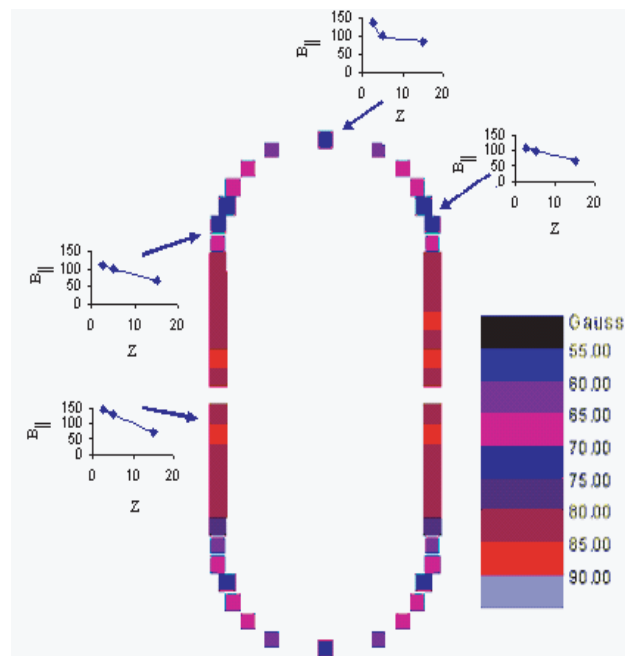


Figure 2. Distribution of the magnetic field component $B_{||}$ measured at a distance of about 1.5 cm from the target surface. The variation of $B_{||}$ in various parts of the race track with the distance from the target surface is shown in the side graphs.

20 kHz with reverse pulse durations of 10 μs , and reverse positive voltage of about 10% of the negative voltage. The current and voltage pulse forms were recorded using a Tektronix[®] TDS 3034 oscilloscope connected to a Tektronix[®] P5205 high voltage differential probe and a Tektronix[®] TCP 202 current probe.

The synchronization of the CCD camera and the pulsed dc discharge was done in the following way: a Tektronix[®] P5200 high voltage differential probe was fed into a BNC Model 555 pulse/delay generator and 5 V TTL trigger pulses were produced. The TTL trigger pulses were then directed to a ST-133 controller to control the electronic shutter of the ICCD camera. The camera was exposed to the discharge for 0.05–0.2 μs with 0.05–2 μs separation between each exposure. When no optical filter is used, the camera integrates the emission intensity in the wavelength region from the near UV (around 250 nm) to the near-infrared (850 nm) and displays the recorded intensity on a relative (not calibrated) scale that ranges from bright red (highest emission intensity) to dark blue (no appreciable emission intensity). An optical filter for the Ar I lines at 750.38 and 751.47 nm (centre wavelength at 752.61 nm and the FWHM of 9.7 nm) was also used to record spectrally resolved images of these Ar lines.

3. Details of the MC simulation

In this section, we present the model used for simulating the plasma emissions at the onset of a voltage pulse. We first briefly describe the ‘standard’ MC model (applicable to a steady state magnetron plasma) and then show how the model can be modified to deal with the case of a rapidly rising voltage pulse.

3.1. Standard MC model

A detailed description of the standard MC model used here can be found in [32]. We will only give a brief summary. The electron motion in the magnetron discharge can be calculated by solving the Lorentz equation:

$$\frac{d\bar{v}}{dt} = \frac{q}{m}(\bar{E} + \bar{v} \times \bar{B}), \quad (1)$$

with q , m and \bar{v} being the charge, mass and velocity of the electron, respectively. To solve this equation, both the magnetic (\bar{B}) field and electric (\bar{E}) field are needed. The magnetic field is calculated analytically by introducing magnetic charges [33]. In the retracing step, only the secondary electrons (SE), i.e. the electrons emitted from the target surface due to ion bombardment are retraced.

We apply the fourth-order Runge–Kutta method with a fixed time step Δt to solve the Lorentz equation. The collision probability p_{coll} during that time step for an electron with energy E_0 is given by:

$$p_{\text{coll}} = 1 - \exp[-\Delta s n_g \sigma(E_0)], \quad (2)$$

where Δs is the distance travelled in Δt , n_g refers the neutral gas density and $\sigma(E_0)$ denotes the collision cross section. A random number RN is generated and compared with p_{coll} . If $RN > p_{\text{coll}}$, no collision occurs and the electron simply continues on its trajectory. If $RN < p_{\text{coll}}$, an electron interaction occurs. For the electron interactions considered here (ionization, excitation and elastic

collisions), we use the cross-sections of Bretagne *et al* [34]. When an electron interaction occurs, another random number is generated to determine the type of interaction and the electron velocity vector is changed accordingly by first adjusting its magnitude, i.e. the electron energy. In case of an elastic collision, the energy transfer is very small and can be neglected. For an excitation, the electron energy is reduced by 12 eV reflecting the fact that most excitations lead to the lowest-lying excited manifold of the Ar energy levels [27]. For an ionization event, both the energy of the incident electron and the ejected electron must be determined. The energy E_{eject} of the ejected electrons is taken as 10 eV [35]. Given the ionization energy E_{ion} (16 eV) of Ar, the electron energy E after an ionization is given by:

$$E = E_0 - E_{\text{ion}} - E_{\text{eject}}. \quad (3)$$

In addition, the orientation of the velocity vector of the electron must be adjusted. For the axial scattering angle, we implemented the expression proposed by Okhrimovskyy [36]. The azimuthal scattering is assumed to be isotropic.

The set of required input parameters for the MC model consists of the gas pressure, the magnetic field, the discharge voltage, and the cathode sheath thickness. The first three input parameters can be obtained directly from the experimental observations, for the latter a value typical for a magnetron discharge is assumed. This steady state value of the cathode sheath thickness d_{SS} combined with the discharge voltage allows us to determine the electric field under the assumption that the electric field is linear within the sheath.

3.2. Modification of the standard MC model

The standard MC model described above must be modified to be applicable to the specific conditions during the onset of a fast-rising voltage pulse. We assume that the simulation is only valid for a short time interval $[0, t_1]$ during the rise time of the voltage pulse ($t_1 \ll t_p$ where t_p is the total width of the pulse). This allows some necessary simplifications. The changes to the standard MC model affect the discharge voltage, the cathode sheath thickness, the starting positions of the retraced electrons, and the time frame during which electrons are retraced.

3.2.1. The discharge voltage. As mentioned before, the discharge voltage is part of the set of input parameters of the simulation. At the beginning of a pulse, the discharge voltage is ramped up as can be seen in figure 3 (see below). Consequently, the discharge voltage during the simulation is not kept constant, but the experimentally measured time dependence of V_d is used as an input parameter.

3.2.2. The cathode sheath thickness. The cathode sheath thickness is another required input parameter for the simulation. Experimental observations show that at the end of the ‘off-time’, the density of charged particles is not zero [18, 37]. A thin anode sheath is formed at the target [38]. At the beginning of the ‘on-time’, in the first few nanoseconds, an ion matrix cathode sheath is formed. During the following period of the order of the inverse ion plasma frequency, ion movement results in the expansion of the sheath [39]. At this time, the formation of the sheath, and thus also its thickness, is additionally controlled by an increase of both the plasma density (decreasing thickness) and the cathode voltage (increasing thickness). The increase of the plasma density by many orders of magnitude justifies the assumption that the initial cathode sheath thickness d_{start} should be much thicker than the steady state cathode sheath thickness d_{SS} .

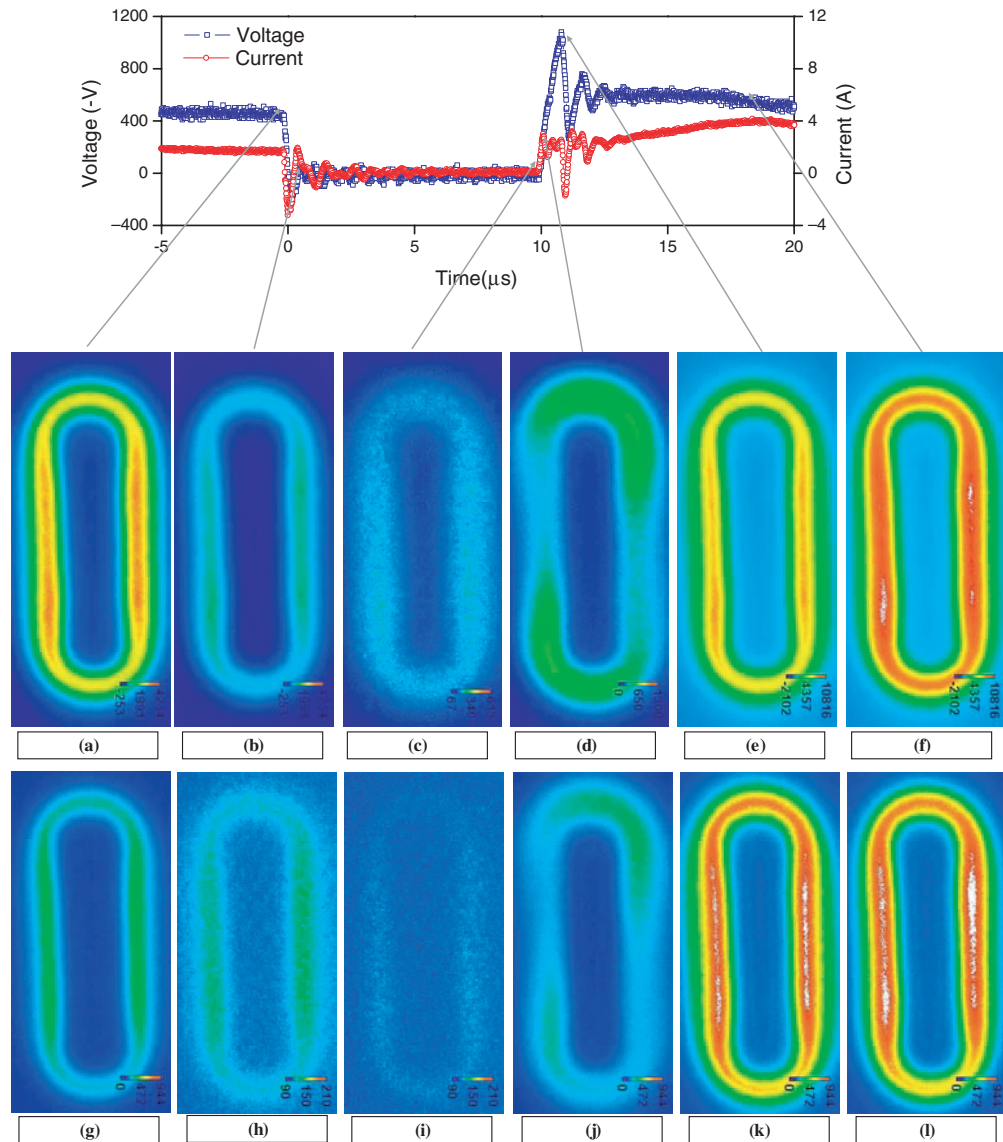


Figure 3. Time-resolved plasma emission images of the race track areas measured without (a)–(f) and with (g)–(l) Ar filter at different times during the pulsed dc power cycle. (The scale is arranged differently in different images for clarity of presentation.)

The MC model is not self consistent and thus cannot be used to simulate this sheath formation process. Instead, the model requires the electric field as an input parameter. Because of a lack of experimental data for this sheath formation process, we assume the sheath to be constant during the time that the electrons are retraced. The electric field within this initial sheath is assumed to be linear, similar to the steady state situation.

3.2.3. The starting position of the retraced electrons. In the standard MC model, the simulation can be started using an arbitrary emission profile of the SE (see e.g. [27]). From the ionization

distribution that is obtained, a new SE emission profile can be deduced. A steady state is reached (and the simulation can be stopped), when the SE emission profile deduced from the simulated ionization distribution is identical to the previous SE emission profile. This yields a self-consistent SE emission profile.

This technique cannot be used here, because we are dealing with a transient phenomenon. Moreover, it is predominantly the slow ‘bulk’ electrons that ‘survive’ the ‘reverse-time’ and that generate the excitation events at the start of the voltage pulse. At the start of the voltage pulse, the cathode sheath thickness d_{start} is large. All electrons within the initial cathode sheath will be accelerated and, as a result, one has to consider the contribution of all these electrons. However, no experimental data are available that can be used as the input distribution for the starting electrons. The simulation of this profile at the end of the ‘reverse-time’ is beyond the scope of the present study. Instead, at the end of the ‘reverse-time’, the electron density is assumed to be constant above the region that corresponds to the steady state race track.

3.2.4. The time frame for retracing the electrons. In the standard MC model, an electron emitted from the target is followed until its energy drops below the threshold for excitation and ionization. The bulk ionization caused by the different electrons is the sum of all ionization events of all electrons. The point in time at which an electron is emitted is not relevant as a steady state situation is considered.

In our case, the situation is fundamentally different, because we want to simulate the optical emissions at a certain time after the start of the voltage pulse. As mentioned before when discussing the starting position of the electrons, we assume that the excitations at the onset of a voltage pulse are caused by the electrons that survived the ‘reverse-time’ period. Hence, these electrons need to be retraced. This implies that all the electrons that are retraced can be followed starting from the same point in time, i.e. from the starting point of the pulse ($t = 0$). This is an approximation, because in reality ions will bombard the target during the time the electrons are retraced. This will lead to the emission of SE, which will be accelerated into the plasma and contribute to the plasma formation. However, the ions take a relatively long time to reach the target, so that during the short time that the electrons are retraced, this effect can be neglected. However, this implies that our model is only valid for a very short time after the onset of the voltage pulse (less than $1 \mu\text{s}$).

When a picture is taken of the optical emission at a time t_{obs} , the light is gathered during a time interval $\delta t_{\text{exp}} = 0.05\text{--}0.2 \mu\text{s}$. To mimic this exposure time in the simulation, the situation at t_{obs} is represented by adding together all excitation events during the time interval $(t_{\text{obs}} - 0.1 \mu\text{s}, t_{\text{obs}})$.

4. Results

Here we present first the results of the experimental studies followed by the results of the MC simulation.

4.1. Experimental results

Figure 3 shows two series of plasma images recorded at different points in time during the pulsed dc cycle, without any filter (a)–(f) and with an Ar filter (g)–(l). Both series of images show very similar results indicating that the dominant emission in the spectral region covered by the camera

consists mainly of emission of Ar and to some degree of emissions of O. Both emissions are mainly due to the collisional excitation of ground state Ar and O atoms by electrons, which require minimum energies of more than 10 eV [14].

The images (a) and (g) in figure 3 are recorded at the end of the ‘on-time’ and represent the emission distribution of a steady state plasma. The observed emission pattern is similar to what one can expect for a dc magnetron plasma under the same discharge conditions. The optical emissions are more intense along the straight sections of the race track compared to the curved sections indicating a higher plasma density along the straight sections. The plasma density in the race track area depends on the value of the component of the magnetic induction parallel to the target surface B_{\parallel} , and, therefore, is strongly correlated with the magnetic field distribution (figure 2). The magnetic field component B_{\parallel} is stronger in the straight sections than in the curved sections by about 20 Gauss (figure 2).

The temporal variations of the plasma images with the Ar filter in place are similar to the temporal behaviour of the time-resolved optical emission intensity of the Ar I 750.39 nm that was measured earlier using a combination of a spectrometer and the ICCD camera and an aperture that allowed the integration of the emission intensity from the major part of the race track plasma [14]. In both cases, when the cathode voltage is switched from a negative value to a small positive value (at the beginning of the ‘reverse time’), the emission decays initially by about half an order of magnitude in less than 1 μ s (figures 3(b) and (h)) and then decays much more slowly until it reaches almost zero (figures 3(c) and (i)). The initial fast decay of the plasma emissions has been attributed to the rapid loss of the highly accelerated SE (which are often referred to as fast ‘beam’ electrons) at the beginning of the ‘reverse time’, while the subsequent slow decay is due to the bipolar charge carrier diffusion to the walls of the reaction chamber, which results in a slow decrease of both the plasma density and the electron temperature [14, 18]. The emission intensity distribution along the race track at the end of the ‘on-time’ and during the ‘reverse time’ is about the same showing the most intensive emission along the straight sections of the race track. At the beginning of the on time, for less than 1 μ s, the plasma emission distribution is quite different. The emissions from the curved regions of the race track are stronger than those from the straight section (figures 3(d) and (j)). However, this distribution does not persist. The image quickly (within another fraction of a microsecond) shows again the emission distribution that is typical for the steady state, that is, the most intense region is along the straight sections of the race track (figures 3(e) and (k)). During the rest of the ‘on-time’, the emission distribution, in general, remains the same, except that the overall emission intensity continues to increase for a few microseconds and then follows the variations in the cathode current.

In an effort to elucidate the origin of the PER effect observed in our experimental studies, we used the MC approach described earlier to simulate the optical emissions from our pulsed dc magnetron plasma with particular emphasis on the very beginning of the applied voltage pulse. These results will be presented in the next section.

4.2. Results from the MC simulation

We used an analytical model for the magnetic field calculation in an effort to design a ‘virtual’ magnet configuration that mimics the real configuration. As a consequence, the simulated B -field distribution is very close to the experimental distribution shown in figure 2. The magnetic field orientation is such that the electron $E \times B$ drift is clockwise. The simulation results for the excitation processes that are the source of the optical emissions were obtained at a pressure of

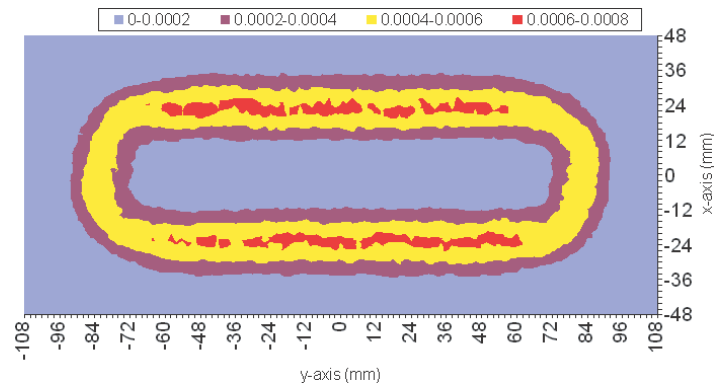


Figure 4. Relative distribution of the excitations simulated using the steady state conditions.

1.2 Pa (neutral gas temperature 300 K) in accordance with the experimental conditions. The time step Δt (required for solving the Lorentz equation) was set to 2×10^{-11} s. For each plot at least 3×10^4 electrons were retraced.

4.2.1. Simulation of the steady state situation. For the steady state situation, the standard MC model was used. The discharge voltage was taken as -500 V based on the experimental results. The cathode sheath thickness d_{ss} was estimated to be 2.0 mm. Figure 4 shows the result for the excitation distribution under steady state condition. In agreement with the experimental observations (figure 3(a)), the emission intensity is highest in the straight part of the magnetron race track.

4.2.2. Simulation of the onset of a fast-rising voltage pulse. For the simulation of the plasma emission at the onset of a fast-rising voltage pulse, the modified MC model as described earlier was used. The time evolution of the discharge voltage as experimentally observed was used as an input parameter (see figure 3). Electrons were started at $t = 0$. Figure 5 shows the excitation events at $t_{obs} = 0.1 \mu s$ for electrons that start 1 mm above the target surface ($z = 1$ mm) for four initial cathode sheath thicknesses, $d_{start} = 4, 6, 8$ and 10 mm. These results show the relative distribution of the simulated Ar emission from direct electron impact. Consequently, these results can be compared with the experimentally obtained Ar emission intensities at 750.38 and 751.47 nm. The simulated excitation distributions show that the preferred emission from the curved regions does not occur for every value of d_{start} . A comparison of these results with the experimental data shows that a value of $d_{start} = 6$ mm as the initial cathode sheath thickness is probably the closest to the experimental situation.

Using $d_{start} = 6$ mm, the excitation distribution was calculated at $t_{obs} = 0.1, 0.2, 0.4$ and $0.6 \mu s$ for electrons starting 1 mm above the target surface (figure 6). These results show the time evolution of the emission distribution and compare well with the experimental data (see figure 3(c)).

Figure 7 shows the excitation distribution at $t_{obs} = 0.1 \mu s$ and $d_{start} = 6$ mm for electrons starting at $z = 0$ and 2 mm above the target surface. Clearly, also for electrons originating from 0 and 2 mm above the target, the emission intensity comes predominantly from the curved regions of the race track, similar to the case $z = 1$ mm. Note that the total number of excitations caused

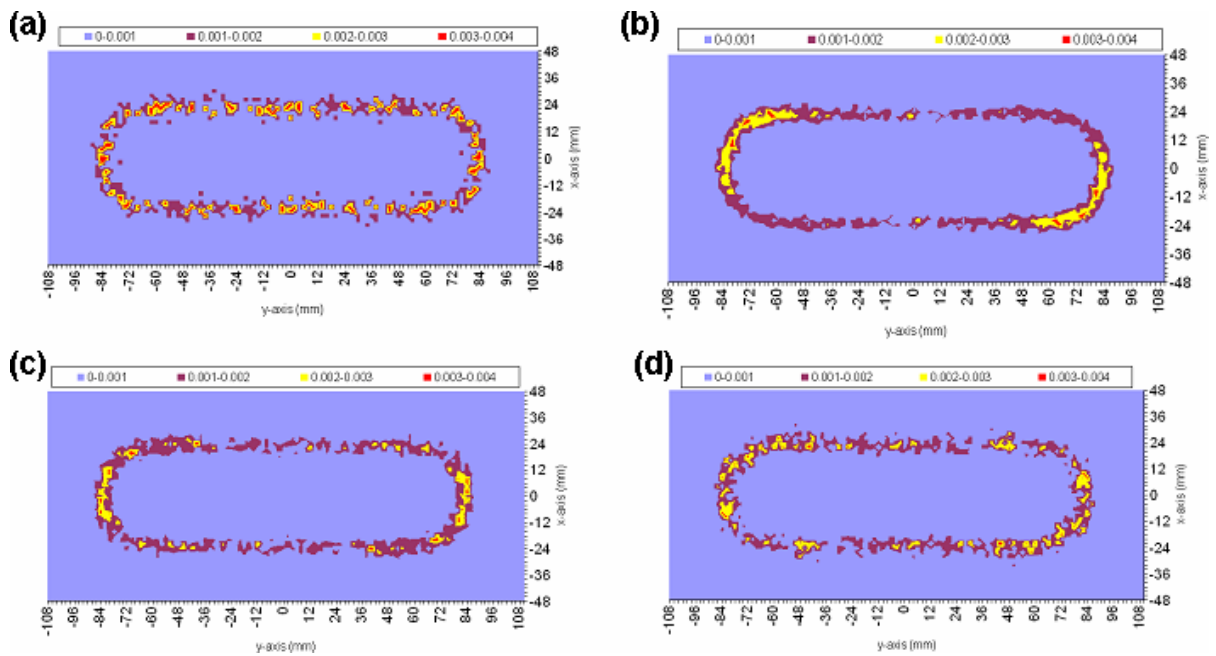


Figure 5. Relative distribution of the excitations at $t_{\text{obs}} = 0.1 \mu\text{s}$ for electrons starting at $z = 1 \text{ mm}$ and sheath thickness d_{start} equal to 4, (a); 6, (b); 8, (c) and 10 mm, (d).

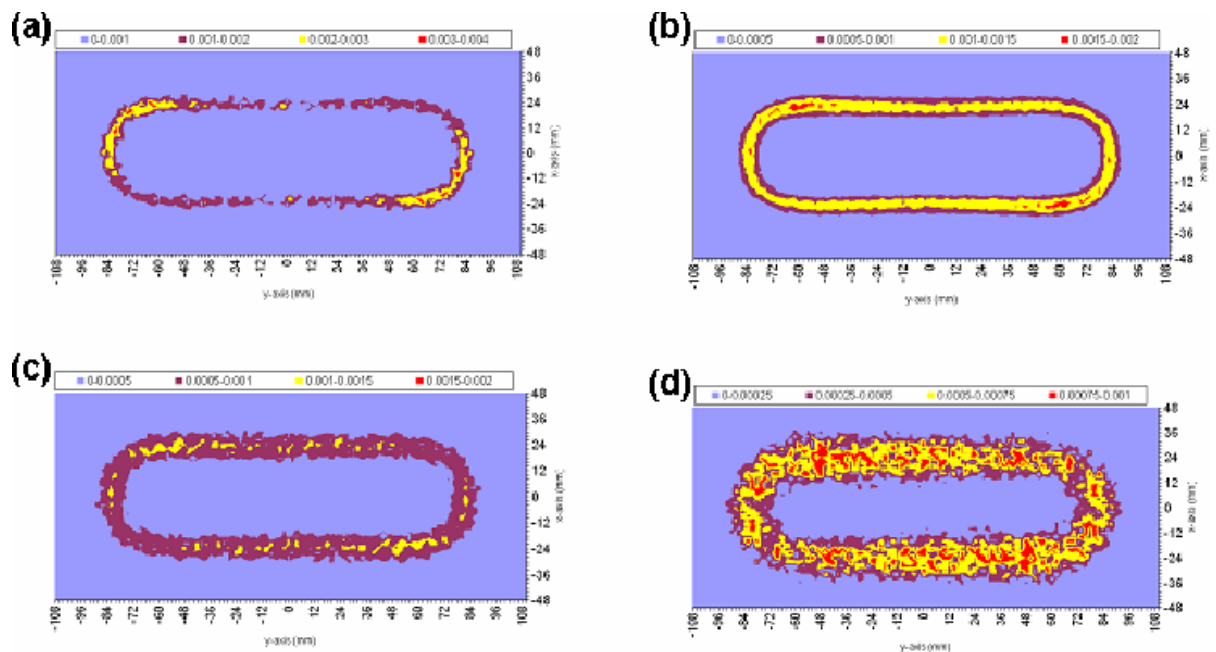


Figure 6. Relative distribution of the excitations at $t_{\text{obs}} = 0.1$ (a), 0.2 (b), 0.4 (c) and 0.6 μs (d) for electrons starting at $z = 1$ and sheath thickness $d_{\text{start}} = 6 \text{ mm}$.

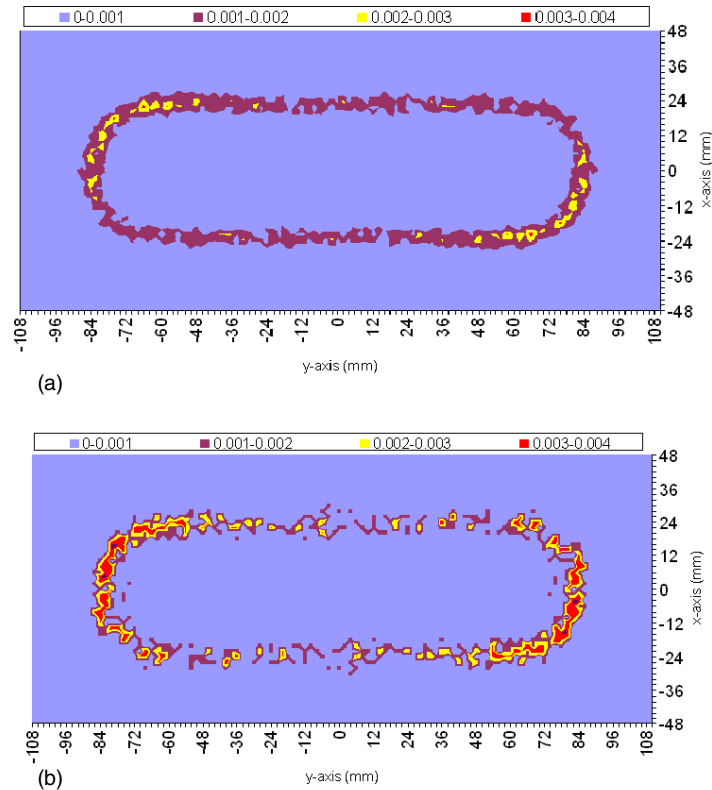


Figure 7. Relative distribution of the excitations at $t_{\text{obs}} = 0.1 \mu\text{s}$ for electrons starting at $z = 0$ (a) and 2 mm (b) and sheath thickness $d_{\text{start}} = 6 \text{ mm}$.

by an electron decreases with increasing starting height. The reason is that the maximum kinetic energy of an electron that originated from a higher starting point above the target is lower.

5. Discussion

Combining the experimental data with the simulation results, we are now in a position to explain the PER effect. We consider two different starting positions on the magnetron target, P_1 and P_2 . P_1 represents a starting position in the straight section of the race track and P_2 denotes a starting point in the curved region of the race track.

5.1. The early stage of a fast-rising voltage pulse

At the start of the voltage pulse the cathode sheath d_{start} is large because of the low charged particle density and the low current density (as mentioned before). Moreover, the discharge voltage V_d is initially very low and, as a consequence, the electric field is weak. This fact in conjunction with the magnetic field distribution prevents the electrons from moving far above the target surface, i.e. they are confined to a place where they cannot gain much kinetic energy and, consequently, cannot excite the emitting Ar or O levels. As the voltage increases, the first places where the electrons gain sufficient energy to cause excitations are places that are at a certain height above the target surface. The height that the electrons can reach is determined by the magnetic field

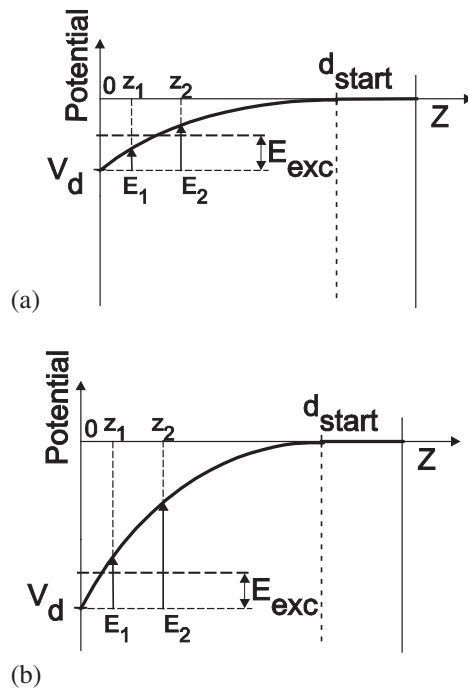


Figure 8. Sketch showing the kinetic energy gain of the SE emitted from the target. Let P_1 be the starting position in the straight section and P_2 the starting position in the curved region. The height that these electrons can reach is given by z_1 and z_2 , respectively, and the corresponding kinetic energies are E_1 and E_2 . Panel (a) shows the situation shortly after the onset of the voltage pulse when V_d is still small, panel (b) shows the situation some time later.

for a fixed electric field. The weaker the magnetic field, the higher the electrons can move above the target surface. The magnetic field distribution (figure 2) shows that an electron emitted in the curved region (P_2) will be able to move higher above the target at the very beginning of the voltage pulse than an electron in the straight section (P_1) due to the smaller magnetic field in the curved section (see figure 2). Let us assume that after a certain time t_{obs} the height of the electrons are z_1 and z_2 for P_1 and P_2 , respectively.

In figure 8, these heights z_1 and z_2 are indicated together with the corresponding kinetic energies E_1 and E_2 for two different values of t_{obs} . Figure 8(a) shows the situation immediately after the onset of the voltage pulse when V_d is still small. As a consequence, an electron emitted at P_1 cannot gain enough kinetic energy to overcome the threshold energy for excitation E_{exc} but an electron at P_2 does. This explains why in figures 6(a), 3(d) and 3(j), the optical emission originates predominantly from the curved regions. Figure 8(b) shows that some time later, due to the increase in V_d , a SE gains sufficient kinetic energy to overcome E_{exc} regardless of its starting position. This corresponds to the situation shown in figures 3(e), 3(k) and 6(d). Optical emissions can now be observed from all race track positions.

When drifting from a weak to a strong magnetic field, the average height of an electron above the target increases [27, 40]. Such a transition from a weak to a strong magnetic field is experienced by electrons when they drift from the curved regions of the race track into the straight parts (see figure 2). Moreover, it has been shown [27, 40] that the electron $E \times B$ drift

velocity decreases because of such a transition. This is also reported in [24, 26] and it is, in fact, the reason for the so-called ‘cross-corner’ effect. Note that in the cited references, the results were obtained in the steady state regime, but as it is the magnetic field gradient that causes this behaviour, the results are also valid for the situation here, i.e. at the onset of a fast-rising voltage pulse. This explains the asymmetry observed in the emission pattern. Because of the $E \times B$ drift, there is an enhanced emission in the region where the electrons drift into the straight part of the race track. Note that according to the results shown in figure 5, the preferred emission from the curved region for a given t_{obs} only occurs for certain cathode sheath thicknesses, d_{start} . The simulation results reveal also that other d_{start} values can result in preferred emissions from the curved regions, but at different t_{obs} values (this is not shown here).

The effect of the redistribution is reproduced here by retracing electrons starting 1 mm above the target surface (see figure 6). Figure 7 shows that also electrons starting from $z = 0$ or $z = 2$ mm display the preferred emission from the curved regions. In reality, electrons will be accelerated from different heights above the surface. Hence, for a more accurate simulation, electrons emitted from different heights above the target surface should be retraced simultaneously.

5.2. The steady state situation

Now, we consider why the plasma emissions are most intense from the straight part during the steady state, i.e. during most of the ‘on-time’. During this time, all electrons, regardless of their starting position, gain enough energy to excite Ar atoms. Consequently, the advantage of the weak magnetic field to generate excitation is lost. In fact, the excitation (and ionization) density will be comparatively lower in the weaker magnetic field region due to the larger $E \times B$ drift velocity of the electrons. This effect is well known and enables the tuning of the uniformity of the erosion and, consequently, of the deposited film in large area magnetrons [27, 40]. This explains why both the experimental data and the simulation results show a lower emission intensity under steady state conditions in areas where the magnetic field is weak, i.e. in the curved regions. We further note that it has been reported in [27] that increased ionization coincides with enhanced erosion of the target and that this can occur at a transition from a weak to a strong magnetic field.

Lastly, the variation of the brightness of the plasma image during the pulsed dc power cycle follows closely the temporal variations of the emission intensity of Ar and O lines recorded earlier in TR-OES studies that collected the light from the centre of the curved areas of the race track. These variations, discussed in detail elsewhere [14, 18], were also correlated with variations of the plasma properties obtained from time-resolved electrical probe data. No temporal changes in the spatial distribution of the plasma in a plane parallel to the target surface have been considered so far in the analysis of pulsed dc magnetron plasmas. The images recorded in this study show that the spatial plasma distribution along the race track of a planar rectangular magnetron does, however, vary during a single pulse cycle.

6. Conclusions

In this paper, we report experimental data from imaging studies and the results of a MC simulation elucidating the PER effect. By combining the simulation results with the experimental data, the PER effect can be explained as follows: the electrons that are still present in the vicinity of the

target surface at the end of the ‘reverse-time’ are accelerated at the beginning of the ‘on-time’. However, due to the magnetic trapping and the low discharge voltage at the onset of the voltage pulse, only the electrons that can move high above the target surface are able to gain enough kinetic energy to cause excitation of argon atoms at the very beginning of the voltage pulse. Hence, the light emission caused by these excitation processes originates predominantly from regions where the electrons can gain higher kinetic energies, i.e. from the curved regions and from regions where the electrons drift from the curved regions into the straight parts of the race track. As the voltage pulse evolves and the discharge voltage increases, all electrons can gain enough energy for excitation and light emissions will occur from all positions within the race track. The curved regions (where the magnetic field is weaker) will now exhibit a slightly lower emission intensity because the weaker magnetic field results in a lower electron density due to a larger electron $E \times B$ drift.

Acknowledgments

This study was supported in part by the US National Science Foundation (NSF) and by the US Army TACOM/ARDEC under contract DAAE30-00-D-1011 DO#20-1 (Picatinny Arsenal). Partial financial support of this study by the NSF through an AGEP grant to Jose Lopez is also gratefully acknowledged. We acknowledge the technical assistance of Paul I Nippes (Magnetic Products and Services, Inc.) and of Professor E B Brucker (Stevens Institute of Technology). JL further acknowledges a MAC Doctoral Fellowship from the State of New Jersey. The research work of Guy Buyle was financed through a grant from the Institute for the Promotion of Innovation by Science and Technology in Flanders (IWT).

References

- [1] Glocker D A and Shah S I (ed) 2003 *Handbook of Thin Film Process Technology* (Bristol: Institute of Physics Publishing)
- [2] Wasa K, Kitabatake M and Adachi H 2004 *Thin Film Materials Technology: Sputtering of Compound Materials* (Park Ridge, NJ: Noyes Publications)
- [3] Arnell R D and Kelly P J 1999 *Surf. Coat. Technol.* **112** 170–6
- [4] Shon C H and Lee J K 2002 *Appl. Surf. Sci.* **192** 258–69
- [5] Schiller S, Goedicke K, Reschke J, Kirchhoff V, Schneider S and Milde F 1993 *Surf. Coat. Technol.* **61** 331
- [6] Scholl R 1993 *36th Annu. Tech. Conf. Proc. (Dallas)* (Albuquerque, NM: Society of Vacuum Coaters) p 405
- [7] Frach P, Heisig U, Gottfried C and Walde H 1993 *Surf. Coat. Technol.* **59** 177
- [8] Belkind A, Freilich A and Scholl R 1998 *Surf. Coat. Technol.* **108–9** 558
- [9] Kelly P J and Arnell R D 1998 *J. Vac. Sci. Technol. A* **16** 2858
- [10] Bradley J W, Backer U H, Kelly P J and Arnell R D 2001 *Surf. Coat. Technol.* **135** 221–8
- [11] Bradley J W, Backer U H, Kelly P J and Arnell R D 2001 *Surf. Coat. Technol.* **142–4** 337–41
- [12] Bradley J W, Karkari S K and Vetushka A 2004 *Plasma Sources Sci. Technol.* **13** 189–98
- [13] Welzel Th, Dunger Th, Kupfer H and Richter F 2004 *J. Appl. Phys.* **96** 6994
- [14] Belkind A, Freilich A, Lopez J, Zhao Z, Zhu W and Becker K 2005 *New J. Phys.* **7** 9
- [15] Mišina M, Bradley J W, Backer H, Aranda-Gonzalvo Y, Karkari S K and Forder D 2003 *Vacuum* **68** 171–81
- [16] Cornett M, George M, Walde H, Casson L and Pini R 2002 *SVC 45th Ann. Tech. Conf. Proc.* p 335
- [17] Pajdarová A D, Vlček J, Bělský P and Musil J 2003 *Proc. 26 Int. Conf. on Phenomena in Ionized Gases (ICPIG) Greifswald*, vol 1, ed J Meichsner, D Loffhagen and H-E Wagner (Greifswald: Kiebu-Druck GmbH) pp 1139–40

- [18] Lopez J, Zhu W, Freilich A, Belkind A and Becker K 2005 *J. Phys. D: Appl. Phys.* **38** 1769–80
- [19] Wallendorf T, Marke S, May C and Strümpfel J 2003 *Surf. Coat. Technol.* **174–5** 222
- [20] Moiseev T and Cameron D C 2005 *Surf. Coat. Technol.* **200** 644
- [21] Dunger Th, Welzel Th, Welzel St and Richter F 2005 *Surf. Coat. Technol.* **200** 1676
- [22] Swindells I, Kelly P J and Bradley J W 2006 *New J. Phys.* **8** 47
- [23] Lopez J, Zhu W, Freilich A, Belkind A and Becker K 2005 *IEEE Trans. Plasma Sci.* **33** 348
- [24] Shidoji E, Nemoto M and Nomura T 2000 *J. Vac. Sci. Technol. A* **18** 2858
- [25] Lopp A, Braatz C, Geisler M, Claus H and Trube J 2002 *45th SVC Ann. Tech. Conf. Proc.* p 170
- [26] Fan Q H, Gracio J J and Zhou L Q 2004 *J. Appl. Phys.* **95** 6017
- [27] Buyle G, Depla D, De Gryse R and De Bosscher W 2005 *SVC 48th SVC Annual Tech. Conf. Proc.* p 254
- [28] Sheridan T E, Goeckner M J and Goree J 1990 *J. Vac. Sci. Technol. A* **8** 30
- [29] Ido S and Nakamura K 1993 *Japan. J. Appl. Phys.* **32** 5698
- [30] Kubart T, Novak R and Valter J 2004 *Czech. J. Phys. C* **54** C1027
- [31] Richter F, Welzel T, Dunger T and Kupfer H 2004 *Surf. Eng.* **20** 163
- [32] Buyle G 2005 Simplified model for the d.c. planar magnetron discharge *PhD Thesis* Universiteit Gent
- [33] Schabes M E and Aharoni A 1987 *IEEE Trans. Magn.* **23** 3882
- [34] Bretagne J, Calledé G, Legentil M and Puech V 1986 *J. Phys. D: Appl. Phys.* **19** 761
- [35] Bretagne J, Calledé G, Legentil M and Puech V 1986 *J. Phys. D: Appl. Phys.* **19** 779
- [36] Okhrimovskyy A, Bogaerts A and Gijbels R 2002 *Phys. Rev. E* **65** 037402
- [37] Bäcker H and Bradley J W 2005 *Plasma Sources Sci. Technol.* **14** 419
- [38] Chapman B 1980 *Glow Discharge Processes* (New York: Wiley)
- [39] Wood B P *et al* 2000 *Handbook of Plasma Immersion* ed A Anders (New York: Wiley) p 243
- [40] Buyle G, Depla D, Eufinger K, Haemers J, De Gryse R and De Bosscher W 2004 *47th SVC Ann. Tech. Conf. Proc.* p 265